





Article

A Preliminary Study on the Quality of Joining AISI 316 and AISI 3415 Steel by the Near Solidus Forming Process

Gorka Plata ^{1,*}, Olaia Gordo-Burgoa ¹, Jokin Lozares ², Andrea Sánchez ³, Asier Bakedano ⁴, Iñaki Hurtado ¹
and Carl Slater ⁵

¹ Mechanical and Manufacturing Department, Mondragon Unibertsitatea, Loramendi 4, 20500 Mondragon, Spain; ogordo@mondragon.edu (O.G.-B.); ihurtado@mondragon.edu (I.H.)

² Department of Mechanics, Design and Industrial Management, University of Deusto, Avda. de las Universidades 24, 48007 Bilbao, Spain; jokin.lozares@deusto.es

³ Department of Steels and Metallic Alloys, Fundación Idonial, Parque Empresarial PEPA, 33417 Avilés, Spain; andrea.sanchez@idonial.com

⁴ AZTERLAN, Basque Research and Technology Alliance (BRTA), 20850 Durango, Spain; abakedano@azterlan.es

⁵ Warwick Manufacturing Group (WMG), University of Warwick, Coventry CV4 7AL, UK; c.d.slater@warwick.ac.uk

* Correspondence: gplata@mondragon.edu

Abstract: In this study, the Near Solidus Forming (NSF) process, which falls under the umbrella of semi-solid processes, was utilized to coforge an AISI 316 tube and an AISI 3415 rod into an as-forged valve geometry. The billet used for the process was kept as large as possible to increase the contact surface area between the two materials. The process was carried out at 1360 °C in a single stroke, almost completely filling the geometry. No joining was observed in areas where low strains were expected, but in regions with medium to high strains, cross-diffusion of 2–7 μm was observed. The presence of small oxide particles was also observed in the joint due to the bimetallic billet shape.

Keywords: stainless steel; NSF; diffusion; joining; biomaterial; semi-solid; coforging



Citation: Plata, G.; Gordo-Burgoa, O.; Lozares, J.; Sánchez, A.; Bakedano, A.; Hurtado, I.; Slater, C. A Preliminary Study on the Quality of Joining AISI 316 and AISI 3415 Steel by the Near Solidus Forming Process. *Metals* **2023**, *13*, 1230. <https://doi.org/10.3390/met13071230>

Academic Editors: Frank Czerwinski and Alfonso Paoletti

Received: 15 May 2023

Revised: 23 June 2023

Accepted: 26 June 2023

Published: 4 July 2023



Copyright: © 2023 by the authors. Licensee MDPI, Basel, Switzerland. This article is an open access article distributed under the terms and conditions of the Creative Commons Attribution (CC BY) license (<https://creativecommons.org/licenses/by/4.0/>).

1. Introduction

Semi-solid-state processes originated from the discovery of thixotropy in metals when liquid and solid phases coexist [1]. With the application of shear stresses, the material undergoes a drastic reduction in strength, facilitating its ability to be molded. However, if the material is left at rest for a period of time after exerting these forces, it returns to its initial conditions [2]. Thanks to this phenomenon, various manufacturing processes were developed to take advantage of this material behavior, achieving components with better mechanical properties than those obtained by high-pressure die casting (for example) while maintaining similar tonnage levels [3].

However, this phenomenon is only real at low solid fractions (<50–60% depending on the alloy and microstructure). At high solid fractions (>60%), the material still shows a reduction in the necessary stresses for deformation, but the liquid is no longer able to completely fill the areas where the solid has left space, creating intergranular cracks [4,5]. Under these conditions, the material exhibits granular behavior, where the grains undergo decohesion and tend to form deformation bands that are either filled with liquid or remain as cracked areas [6,7]. Performing the process under these conditions allows for better mechanical properties that are closer to forging processes than more typical casting processes [8].

Under this context, various authors have used semi-solid-state processes to manufacture bimetallic components of similar [9,10] and dissimilar alloys [11–13]. In most cases, one of the materials was in solid conditions while the other was heated to semi-solid conditions. The material that remained at solid conditions could be heated [10,13] or left at

room temperature [9,12]. For example, in the case of Liu et al. [13], a 1Cr18Ni9Ti stainless steel was hybridized with the aluminum alloy AlSi7Mg. In this work, both materials were heated to the working temperature defined by the aluminum. It was observed that the best conditions were at the temperatures at which the aluminum had a solid fraction of 30%, conditions in which the best shear properties were recorded. Other authors have also reached the same conclusion [10,14], so it seems that, in the case of aluminum, that 30% fraction is the ideal condition from a point of view of shear mechanical properties thanks to the diffusion of elements during the process between both materials.

Other authors such as Echániz [12] and Kopp et al. [9] used the base material at room temperature conditions. In these cases, hybridization did not generate any diffusion, nor did it generate intermetallics or oxides between the materials. In these cases, the mechanical properties are given by the mechanical bond between both materials thanks to the fabricated geometry. For example, Kopp et al. [9] used screws that were coated with semi-solid material. Thus, the screw teeth themselves support the stresses, without the need to generate any diffusion of elements. Echániz [12] used a semi-solid aluminum that was injected onto a square steel profile that, during the process, deformed and generated that mechanical bond between both materials.

However, under these conditions, the properties achieved are more similar to those of casting than forging. As previously mentioned, the higher the solid fraction, the better the mechanical properties. This is where the Near Solidus Forming (NSF) process comes into play. The NSF process is a closed-volume forging technique where the material is heated to temperatures near the solidus. This technology represents an advancement derived from semi-solid-state manufacturing techniques, particularly when operating at elevated solid fractions. It maintains identical material behavior while operating in a fully solid state, thereby facilitating the production of complex geometries akin to those achievable through hot forging. The required force is reduced by approximately 8 fold (from a 3500 t press to a 400 t press), the forging steps by 4 fold (from 3 forging strokes plus trimming to a single deformation step in NSF), and the required material by 20% due to the elimination of flash. All of this is achieved while maintaining the as-forged mechanical properties of the components [15].

However, in addition to these benefits, there are many other advantages that can be obtained with this process due to the behavior of the material under these conditions [16]. One of these benefits, which has recently been evaluated, is the ability of the process to co-forge dissimilar materials to produce a complex component. Slater et al. [17] have demonstrated how the NSF process can successfully co-forge AISI 304 stainless steel and 42CrMo4 medium carbon steel to produce a complex geometry with two materials joined by chemical diffusion. They found that a cross-diffusion of elements such as Fe, Cr, and Ni of around 3 μm was observed.

When compared to other solid-state joining processes such as Friction Welding, Friction Stir Welding, or diffusion bonding [18], which are generally limited to simple geometries and where cross-diffusions of around 1–2 μm are found with similar alloys [19], the NSF process shows a great capacity for joining, which needs to be further analyzed and understood before moving on to a real case study. To achieve this, this research will focus on studying the joining capacity of other important steels such as AISI 316 and AISI 3415.

The combination of these two alloys could be interesting in applications where the main requirement of the component is to have excellent corrosion resistance. In such applications, the working area is the surface, and the core is only important to withstand the loads. Thus, the coforging of AISI 316 as an outer surface material and AISI 3415 as a core material combines the great corrosion resistance of the former with the good mechanical properties and reduced cost of the latter. This way, components with the same corrosion properties and, in some cases, better mechanical properties can be achieved at a lower cost by using a cheaper steel with similar or greater mechanical resistance.

To determine the capabilities of this proposal, a preliminary study on the coforging of these two alloys via NSF has been conducted using a valve geometry. Different zones of

the component have been microstructurally analyzed and related to the estimated process conditions according to the performed simulation. As a result, significant cross-diffusion has been identified in different zones, and an initial relationship between temperature, strain, time, and billet shape with the joint quality is given.

2. Materials and Methods

2.1. Materials

The materials utilized in this study are AISI 316 stainless steel and AISI 3415 low alloyed steel. The former is an austenitic stainless steel commonly utilized in applications where the components must endure corrosive environments. As for AISI 3415, it is a low-carbon steel with a low proportion of alloying elements, making the material relatively inexpensive while still having good mechanical properties. As a result, in applications where corrosion resistance is sought, the combination of these two materials could be ideal for reducing component costs while maintaining or even improving mechanical requirements. The chemical composition of each alloy is presented in the following tables (Tables 1 and 2):

Table 1. Typical chemical composition of AISI 316.

C	Mn	Si	Cr	Ni	Mo	S	P
0–0.08	2	0.75	16–18	10–14	2–3	0–0.02	0–0.05

Table 2. Typical chemical composition of AISI 3415.

C	Mn	Si	Cr	Ni	S	P
0.12–0.18	0.3–0.6	0.1–0.35	0.6–0.9	3–3.5	0–0.05	0–0.05

According to the literature [20], the solidus temperature of the AISI 316 alloy is approximately 1420 °C. No information regarding the solidus temperature of the AISI 3415 alloy was found by the authors. Consequently, a thermodynamic analysis was performed using FactSage software (version 8.2, GTT technologies, Herzogenrath, Germany) (Figure 1) and the mean values of Table 2, resulting in an estimated solidus temperature of around 1450 °C.

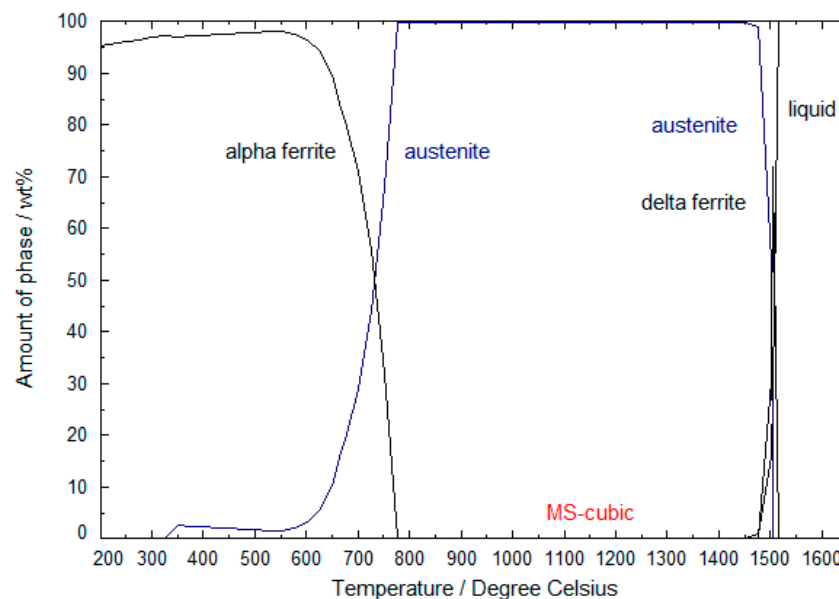


Figure 1. Phases evolution at different temperatures calculated using FactSage software (version 8.2).

This information is crucial for determining the optimal temperature conditions for the Near Solidus Forming (NSF) process involving both materials. It is important to note that in this process, both materials are simultaneously heated, with the outer material (AISI 316) being in the form of a tube that encloses a rod made of the inner material (AISI 3415) (Figure 2). The billet's edges have been manually deformed to prevent displacement between the rod and tube during billet manipulation. Considering that NSF temperatures are typically set at around 95% of the solidus temperature, the selected working temperature for this study will be 1360 °C.

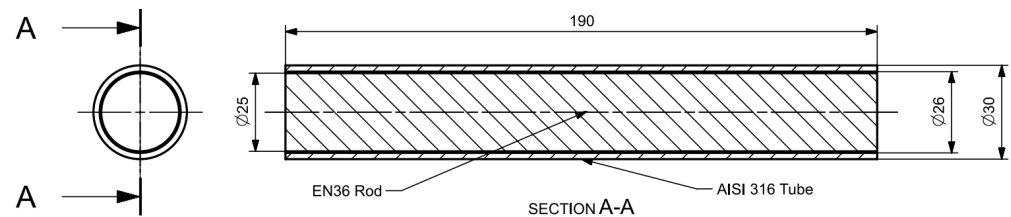


Figure 2. Bimetal billet consisting of an EN36 rod of 26 mm diameter and 190 mm long and an AISI 316 tube of an inner diameter of 26 mm, an outer diameter of 30 mm and 190 mm long. Note that all the dimensions in this figure are in mm.

This billet geometry has been selected for various reasons. The dimensions of the tube and rod allow for a 0.5 mm gap, aiming to investigate whether the presence of air between the two materials could lead to impurity formation in the joint. The length of the rod is 190 mm, which corresponds to the maximum length that the tooling allows for insertion. This configuration maximizes the contact surface between the rod and tube during deformation, compared to billets with larger diameters.

2.2. Geometry

The chosen geometry for this research is an as-forged valve shape with specific modifications (Figure 3). Firstly, additional cavities have been incorporated into the top and right arms to facilitate the escape of lubricant particles. Secondly, a cone shape has been introduced in the upper part of the geometry to accommodate the use of the actual punch of the NSF Cell. As a result of these modifications, the component weighs approximately 1 kg. Although the volume of the billet (Figure 2) is not as large as the cavity of the geometry, resulting in incomplete filling of the component, from a research standpoint, it is more advantageous to maintain the gap and maximize the surface contact between the tube and the rod, as mentioned previously.



Figure 3. Valve geometry with the added cone shaped gate to match the punch diameter.

2.3. NSF Process

The NSF process is conducted in MGEP's NSF cell, which comprises a FAGOR 400 t AC Servo-mechanical press (Fagor Arrasate, Arrasate-Mondragon, Spain) [21], a Hobersal 9-CRN5X-18 muffle furnace (Fons Hobersal, Barcelona, Spain) with a maximum working temperature of 1700 °C, and a custom-designed NSF tooling to ensure closure of the dies during the deformation process facilitated by the upper punch (Figure 4) [15].

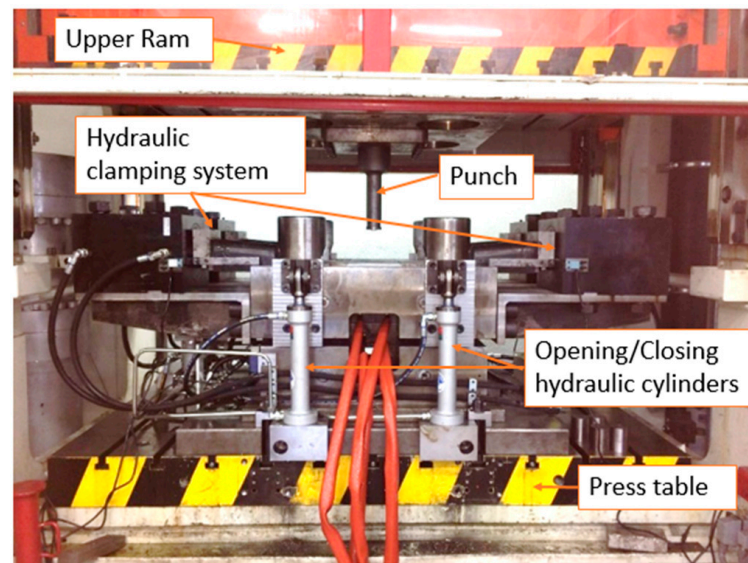


Figure 4. Self-designed NSF tooling for high melting point alloys.

The main difference between the setup designed for this research and the conventional NSF procedure is that, in the present case, the lower die consists of two mechanically closed semi-molds (Figure 5). This enables the fabrication of more complex geometries as we have three dies and the punch simultaneously engaged in the deformation process. Apart from manually opening these two semi-molds to extract the component, the remaining manufacturing steps are identical. It is worth noting that the dies are uniformly heated to 270 °C to minimize material cooling during the process.

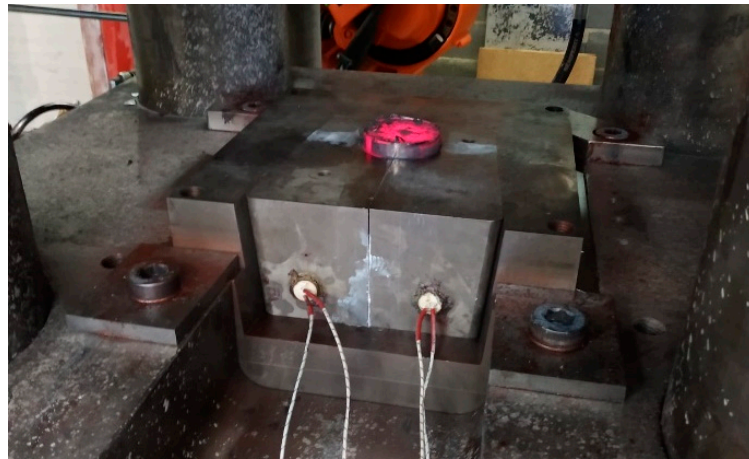


Figure 5. Bottom die holder with the two semi-moulds just after the NSF process. Note that the bottom die holders' dimension is 350 mm × 350 mm × 240 mm.

Taking all of this into account, the steps involved in the NSF manufacturing process are as follows:

- I. Heating the billet in the furnace for 20 min to ensure uniform temperature distribution within the material. An argon flow of 0.5 L/min is used to prevent excessive formation of surface oxide layer.
- II. While the billet is being heated, the dies are cleaned and coated with CeraSpray[®] to reduce the rate of heat transfer between the material and the dies, as well as to act as a lubricant [22,23].

- III. Once the coating is applied and the two semi-molds are placed in the bottom die holder, the tooling is closed, bringing the upper and lower dies into contact, and clamped securely using hydraulic cylinders.
- IV. After the tooling is closed and clamped, and the heating time is completed, the billet is manually removed from the oven and inserted into the tooling through the prepared hole for the punch.
- V. Once the billet is in place, the press moves from the Top Dead Center (TDC) to the Bottom Dead Center (BDC) and returns to the TDC position.

When the press reaches TDC again, the clamping system is retracted, and the dies are separated to extract the component. At this point, the process can be repeated starting from step I.

2.4. Process Simulation

Based on the given inputs, a preliminary simulation will be conducted using FORGE[®] software (version NxT 3.2, Transvalor, Biot, France) to determine the generated strains and/or pressures during the process. To simplify the simulation, a single rod with a diameter of 30 mm and a length of 190 mm made of AISI3415 (14NiCr14 from the FORGE[®] database) will be assumed. The billet geometry will be placed within the 3-die and punch system. The punch will replicate the movement of the press. The objective is to analyze the results obtained from the software and identify approximated areas of interest for subsequent metallographic analysis.

2.5. Microstructural Analysis

Once the component is manufactured and the simulation analysis is completed, samples will be extracted from the most significant areas of interest for microstructural evaluation. The samples will undergo preparation processes, including grinding and polishing, to facilitate examination of the joint quality using a FEI Nova Nano SEM 450 scanning electron microscope (FEI, Hillsboro, OR, USA) (SEM). The SEM is equipped with an Oxford X-max 50 X-ray detector (Oxford Instruments, Abingdon, UK) (EDX) to qualitatively assess the presence and distribution of various alloying elements within the analyzed region.

2.6. Diffusion Simulation

The simulation system will be set up using the Dictra MOBF₅ database, with the length of the previously analyzed microstructure as input. For this simulation, a mean value of the chemical elements shown in Tables 1 and 2 and the cooling rates estimated from the previous process simulation will be utilized as input for the diffusion simulation. Subsequently, a simplified 1D single-phase model will be employed until a temperature of 850 °C, as both alloys retain their austenitic phase up to this temperature.

3. Results

3.1. NSF Process

Once the working temperature is determined, the NSF process is conducted following the defined methodology steps. Figure 6 displays a cross-section of the manufactured component. The maximum load recorded during the manufacturing process of this component was 250 tons.

As shown in Figure 6, there are several areas (highlighted) where the joining process appears to be incomplete. The folds observed in the middle and right sections of Figure 6 are likely a result of billet bending during deformation, possibly due to the high length-to-diameter ratio. In the upper-left zone, the lack of joining may be attributed to the specific processing conditions in that region. The upcoming simulation and microstructural analyses will provide further insights to confirm or better understand the underlying causes.

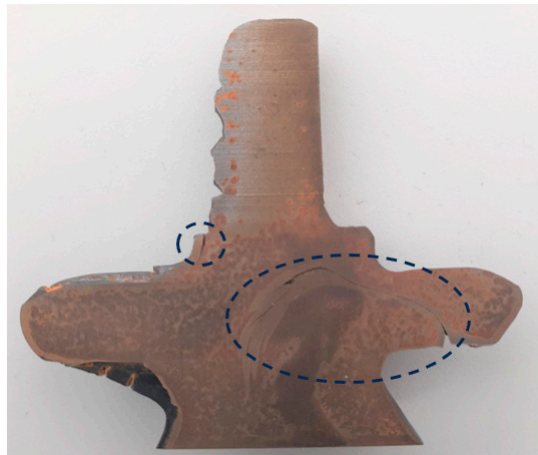


Figure 6. Slice of the valve manufactured via NSF with AISI 316 and EN36 alloys. The highlighted areas are either folds or not joined areas.

3.2. Process Simulation

In the accompanying Figure 7, the deformation progression of the material during the NSF process is illustrated. The simulation successfully predicts the formation of the observed fold in the manufactured component. Initially, as the billet is filled, the rod begins to bend (Figure 7a). Subsequently, as the punch descends, this bending results in the formation of a fold (Figure 7b), which gradually closes and moves downward as the punch continues its motion (Figure 7c). Due to remeshing in the FORGE[®] software (version NxT 3.2), the fold becomes less discernible towards the end of the deformation (Figure 7d), but its creation is evident from the preceding steps.

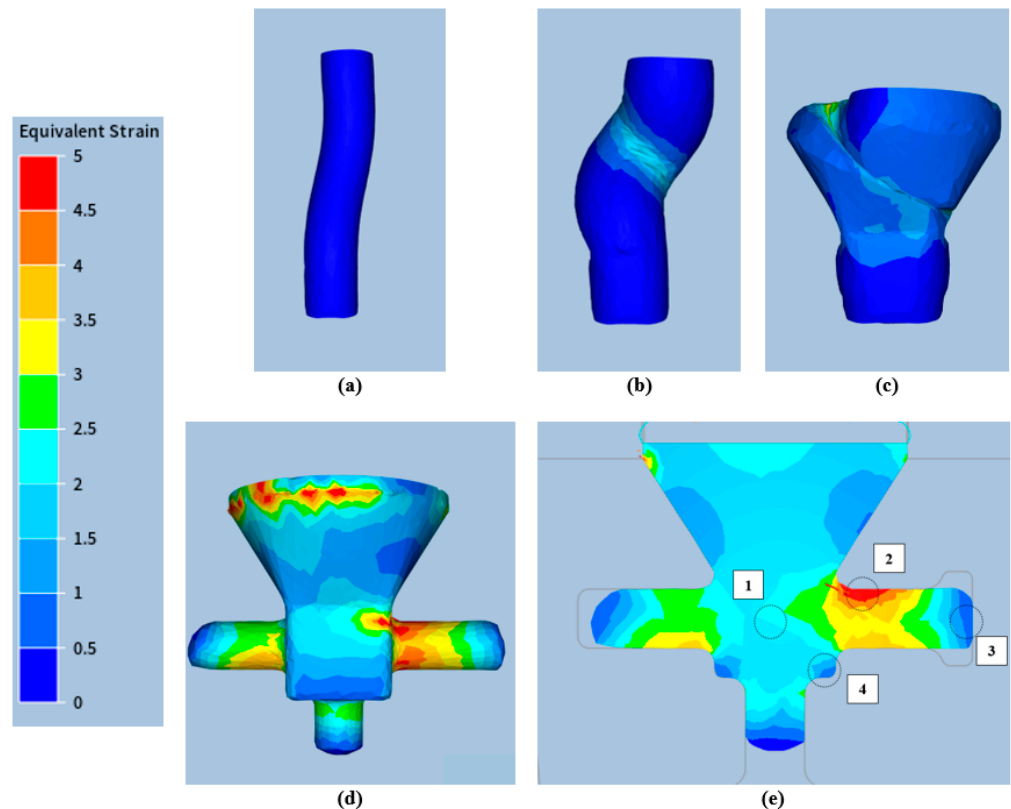


Figure 7. (a–d) FORGE[®] filling simulation results at different punch positions during the NSF process. (e) Map of strains generated in the middle of the component for the conditions shown in (d).

Regarding the filling behavior itself, the actual component (Figure 6) demonstrates better filling in the lower arm compared to the simulation, where filling towards the side arms is more prominent (Figure 7d). It is important to note that this simulation employs a material file tested only up to 1250 °C, indicating that the process calculations rely on extrapolated data, and the boundary conditions may approximate reality, which could account for the filling discrepancy. Additionally, it should be acknowledged that the simulation assumes a fully solid rod, whereas the actual billet is bimetallic. Consequently, the differences in filling may also be influenced by the composition of the billet.

Nevertheless, it is crucial to emphasize that this simulation aimed to identify areas of interest for microstructural analysis rather than replicating the manufacturing process precisely. As demonstrated in Figure 7e, a diverse range of strains is generated in various regions of the component. Some of the most intriguing regions, which will be subjected to microstructural analysis, have been numbered and are defined as follows:

- I. Zone 1 corresponds to the region where the fold has been observed in the manufactured component. Additionally, this area experiences constant pressure, despite the anticipated moderate strains, as the material is compelled to move towards the arms.
- II. Zone 2 encompasses the area where higher strains are anticipated. The material undergoes significant shearing due to a change in deformation direction exceeding 90°.
- III. Zone 3 represents the material that advances forward with minimal deformation.
- IV. Zone 4 pertains to the region where the tube may remain stationary while the rod continues to fill the lower arm. The expected strains are low, and some material displacement between the tube and the rod is anticipated.

3.3. Microstructural Evaluation

In the following figure, the ground and polished samples of the four designated regions are displayed. From these samples, it is already evident that the areas with low strains (Zones 3 and 4) have not achieved a satisfactory joining. Likewise, the folded region highlighted in Zone 1 does not appear to have properly reconnected with AISI 316. However, the areas in contact with AISI 3415 exhibit a good joining. Similarly, the upper part of Zone 2, which experienced the highest strains, also appears to have achieved a proper joining.

Hence, these two regions have been subjected to a comprehensive compositional analysis using SEM to validate the quality of the joints (Figure 8). In this analysis, the two materials can be clearly distinguished, indicating a satisfactory joining. However, numerous oxide particles are observed along the joining surface, likely formed due to the presence of air between the two samples during heating (refer to Figure 2). Regarding the joint quality, the measured cross-diffusion for Zone 1 is approximately 6–7 µm (Figure 9), while for Zone 2, it is around 2 µm (Figure 10).

3.4. Diffusion Simulation

The diffusion simulations of Cr in Zones 1 and 2 are presented in Figures 11 and 12, respectively. It can be observed that the predicted diffusion profile of Cr in Zone 2 aligns well with the measured diffusion results. However, there is a slight disparity between the estimated diffusion profile of Cr in Zone 1 and the measured results. This discrepancy could potentially be attributed to the cooling rate pattern implemented in DICTRA specifically for this zone. It is possible that the simulated cooling rate is faster than the actual rate, which could account for the difference in the diffusion slope. Nevertheless, despite the variation in the mean values of Cr content used in the simulation compared to the measured values, the simulated diffusion results closely replicate the diffusion distance. Thus, this validated simulation setup has been employed to estimate the diffusion of C in these alloys. Figure 13 illustrates the estimated C diffusion for Zones 1 and 2, which amounts to approximately 6 µm and 2–3 µm, respectively.

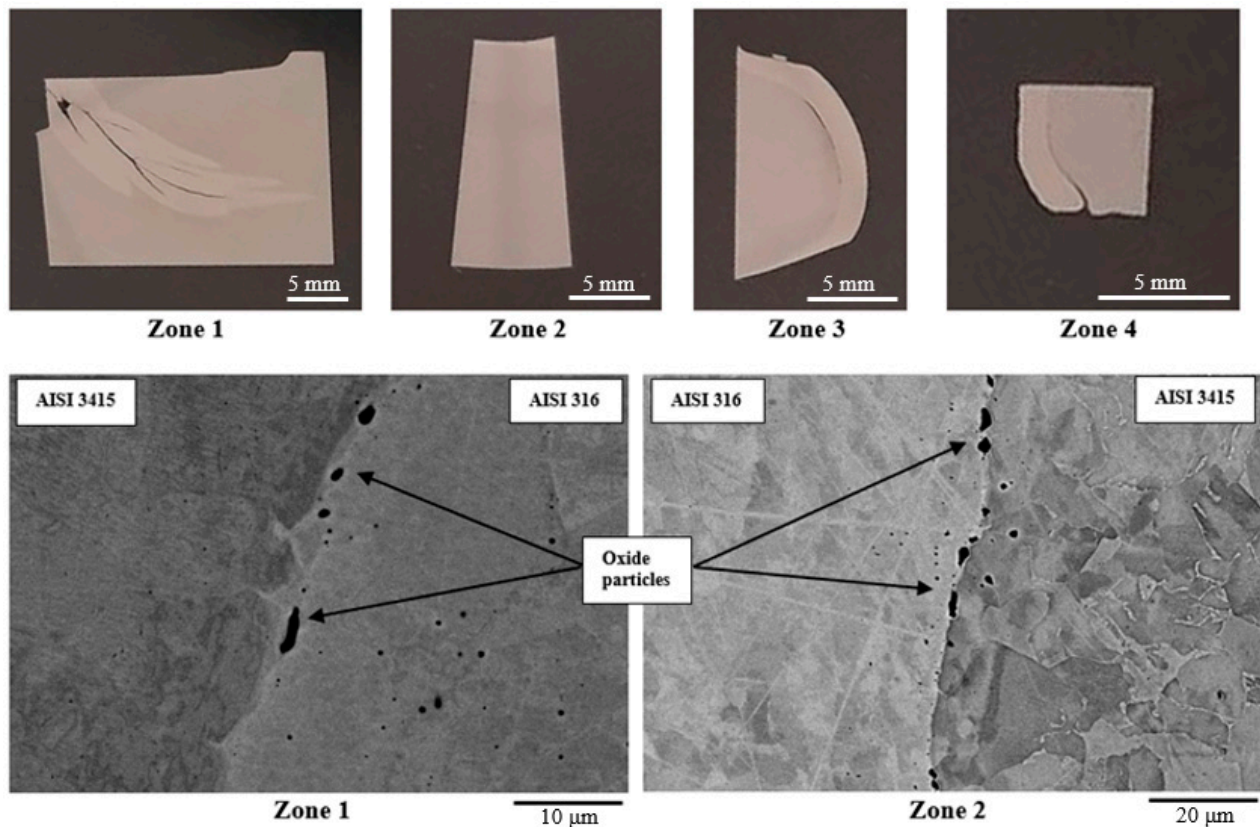


Figure 8. Grinded and polished samples taken from the zones highlighted in Figure 7e and SEM micrographs of the joints of Zone 1 and Zone 2.

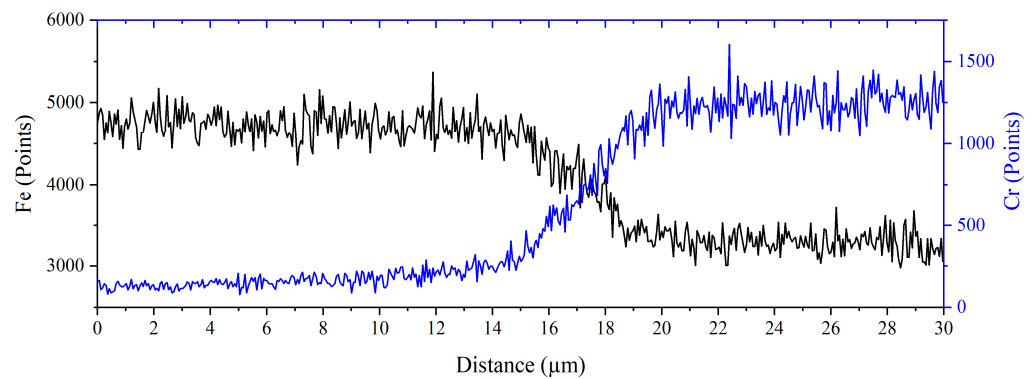


Figure 9. Chemical diffusion of Fe (black) and Cr (blue) results from Zone 1 of the component.

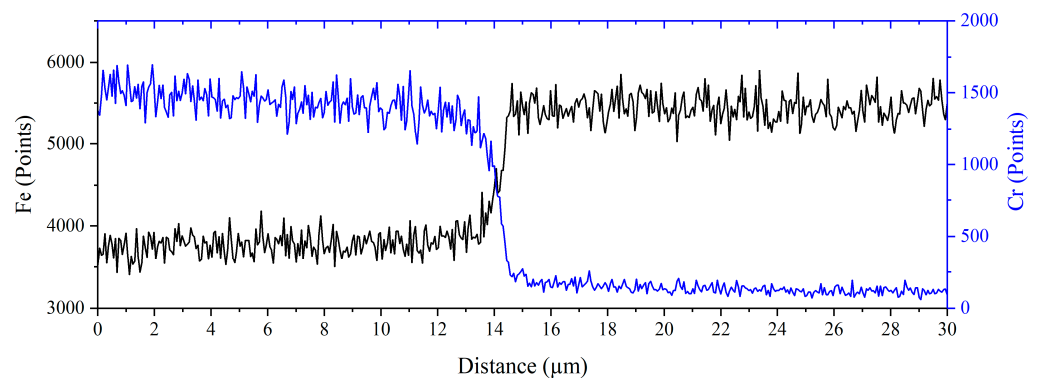


Figure 10. Chemical diffusion of Fe (black) and Cr (blue) results from Zone 2 of the component.

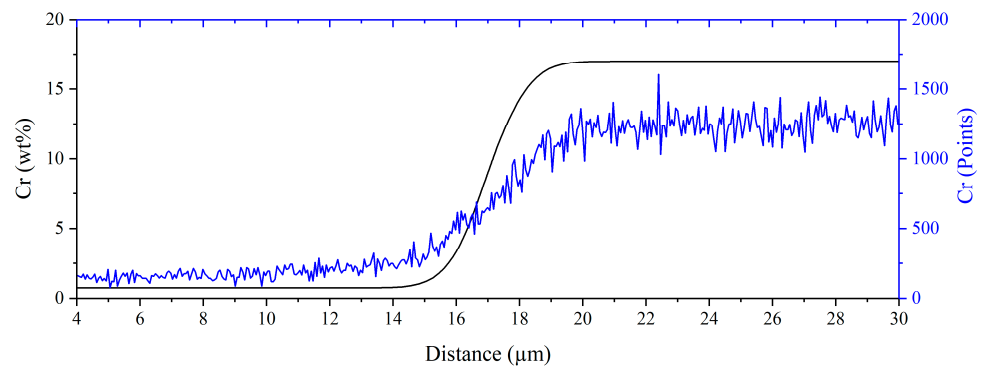


Figure 11. Measured (blue) and simulated (black) chemical diffusion of Cr results for Zone 1 of the component.

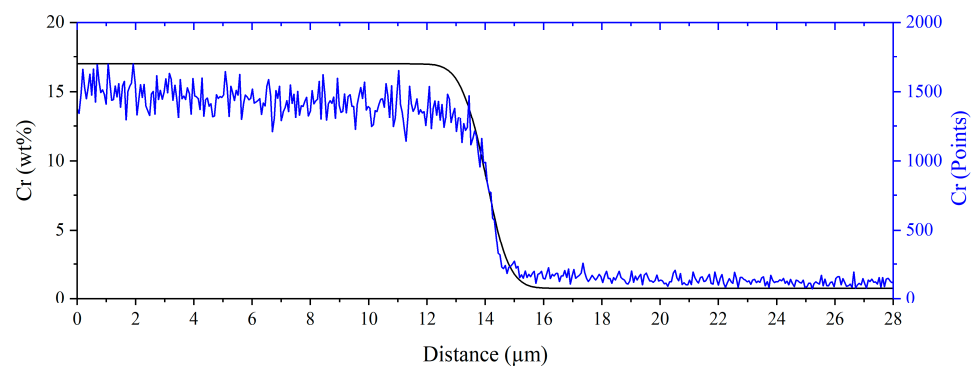


Figure 12. Measured (blue) and simulated (black) chemical diffusion of Cr results for Zone 2 of the component.

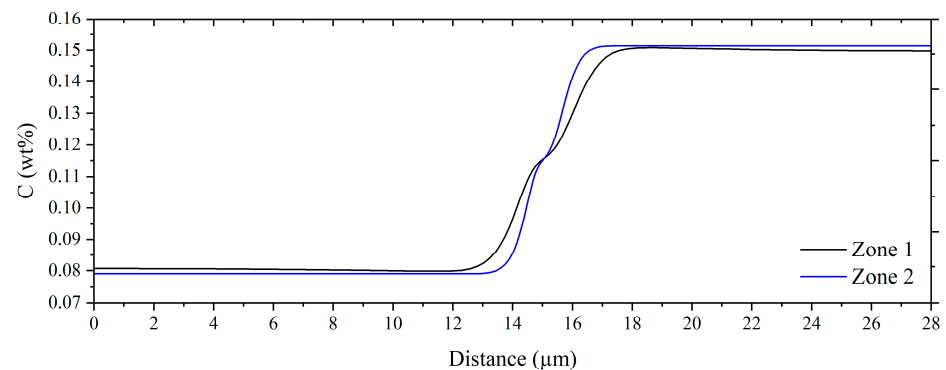


Figure 13. Results of simulated C chemical diffusion in Zone 1 (black) and Zone 2 (blue) of the component.

4. Discussion

According to the results, several interesting outcomes have been identified. Firstly, the generation of oxide particles in the joint seems to be due to the diameter difference between the tube (inner) and the rod, which allows air to enter and oxidize the surface at high temperatures. To prevent this, a higher flow rate of argon should be used, or the gap should be minimized to reduce the amount of air between the two materials.

Regarding joint quality, there are several aspects to highlight. In areas where the strain was low (around or below strains of 1, Zones 3 and 4), the conditions for the two materials to join were not generated. In other areas where this strain level was surpassed (strains above 1.5–2, Zones 1 and 2), chemical diffusion occurred. However, the diffusion depth differed greatly between Zone 1 and Zone 2. Zone 1, where the generated strain is around

2, the measured diffusion was 6–7 μm . In contrast, in Zone 2, where the generated strain was higher than 5, the measured diffusion was 2 μm .

These results suggest that even if some strain is required to ensure minimal contact between the two materials, the time of exposure at elevated temperature is the governing parameter for increasing diffusion. In Zone 1, the material experiences pressurized contact almost from the initial stages, and it retains elevated temperatures for a longer duration compared to Zone 2. This is due to its location in the middle of the component, where heat dissipation occurs at a slower rate. This suggests that to ensure good chemical bonding, the material could be maintained under pressure for a certain period just after the process is finished to increase the pressurized contact time at elevated temperatures and, consequently, promote larger diffusions. This also agrees with the results observed in [16], where, even if it was a single material, the generated folds joined back again at the end of the NSF process. This could also suggest that the observed folds with these two materials could be closed if the entire cavity is filled. However, due to the preliminary nature of this research, these suggestions should be taken as indicative definitions of possible working aspects as further research is required to confirm the proposed solutions.

In reference to the diffusion simulation, the obtained results align with the measured data. By utilizing the same setup, the simulation predicts a cross-diffusion of approximately 6 μm in Zone 1 and 2–3 μm in Zone 2 for carbon, exhibiting a similar behavior to chromium. These findings indicate significant chemical diffusion of carbon, further highlighting the exceptional potential of NSF in creating robust joints and fabricating intricate geometries that surpass those achievable through the conventional Diffusion Bonding or Friction Stir Welding methods.

5. Conclusions

The main conclusions of this work, which involved using an AISI 3415 rod placed into an AISI 316 tube with a 0.5 mm gap between them to manufacture a valve geometry via the NSF process, are as follows:

- Chemical diffusions ranging from 2 to 7 μm have been simulated and observed in different zones. The reason for the difference between zones is still unclear, although it appears that generated strain, pressures, and contact time at elevated temperatures have a significant influence.
- Oxide particles have been observed along the joined surface, likely due to the presence of an air gap between the tube and rod. Minimizing this gap is necessary to ensure optimal joints.
- Various folds have been detected as a result of sample bending. To mitigate this, billets with larger diameter and shorter length should be used.

Author Contributions: Conceptualization, G.P., J.L. and C.S.; methodology, G.P., J.L., A.S. and A.B.; software, O.G.-B. and A.S.; validation, G.P., J.L., A.B. and C.S.; investigation, G.P., O.G.-B., J.L., A.S. and C.S.; data curation, G.P., O.G.-B. and I.H.; writing—original draft preparation, G.P. and O.G.-B.; writing—review and editing, J.L., A.S., A.B., I.H. and C.S.; supervision, A.B., I.H. and C.S. All authors have read and agreed to the published version of the manuscript.

Funding: This research was partially funded by Elkartek program of the Department of Industry, Innovation, Trade and Tourism of the Basque Government, H2MAT project, grant number KK-2022/00064.

Data Availability Statement: Not applicable.

Acknowledgments: The authors want to thank WH Tildesley, specially to Michal and Steven, for their support during this research.

Conflicts of Interest: The authors declare no conflict of interest.

References

1. Spencer, D.B.; Mehrabian, R.; Flemings, M.C. Rheological Behavior of Sn-15 Pct Pb in the Crystallization Range. *Metall. Trans.* **1972**, *3*, 1925–1932. [[CrossRef](#)]
2. Quaak, C.J. Rheology of Partially Solidified Aluminium Alloys and Composites. Ph.D. Thesis, Technische Universiteit Delft, Delft, The Netherlands, 1996.
3. Kapranos, P. Semi-Solid Metal Processing—A Process Looking for a Market. In *Semi-Solid Processing of Alloys and Composites 10—Selected, Peer Reviewed Papers from the 10th International Conference on Semi-Solid Processing of Alloy and Composites, S2P 2008*; Trans Tech Publications: Baech, Switzerland, 2008; Volume 141–143, pp. 1–8. [[CrossRef](#)]
4. Cai, B.; Karagadde, S.; Yuan, L.; Marrow, T.J.; Connolley, T.; Lee, P.D. In Situ Synchrotron Tomographic Quantification of Granular and Intragranular Deformation during Semi-Solid Compression of an Equiaxed Dendritic Al-Cu Alloy. *Acta Mater.* **2014**, *76*, 371–380. [[CrossRef](#)]
5. Karagadde, S.; Lee, P.D.; Cai, B.; Fife, J.L.; Azeem, M.A.; Kareh, K.M.; Puncreobutr, C.; Tsivoulas, D.; Connolley, T.; Atwood, R.C. Transgranular Liquation Cracking of Grains in the Semi-Solid State. *Nat. Commun.* **2015**, *6*, 8300. [[CrossRef](#)] [[PubMed](#)]
6. Gourlay, C.M.; Dahle, A.K.; Nagira, T.; Nakatsuka, N.; Nogita, K.; Uesugi, K.; Yasuda, H. Granular Deformation Mechanisms in Semi-Solid Alloys. *Acta Mater.* **2011**, *59*, 4933–4943. [[CrossRef](#)]
7. Gourlay, C.M.; O’Sullivan, C.; Fonseca, J.; Yuan, L.; Kareh, K.M.; Nagira, T.; Yasuda, H. Synchrotron Radiography Studies of Shear-Induced Dilation in Semisolid Al Alloys and Steels. *Jom* **2014**, *66*, 1415–1424. [[CrossRef](#)]
8. Plata, G.; Lozares, J.; Hurtado, I.; Azpilgain, Z. Semisolid Forging of Steels: Readiness from an Industrial Point of View. *AIP Conf. Proc.* **2019**, *2113*, 140001.
9. Kopp, R.; Kallweit, J.; Möller, T.; Seidl, I. Forming and Joining of Commercial Steel Grades in the Semi-Solid State. *J. Mater. Process. Technol.* **2002**, *130*, 562–568. [[CrossRef](#)]
10. Alvani, S.M.J.; Aashuri, H.; Kokabi, A.; Beygi, R. Semisolid Joining of Aluminum A356 Alloy by Partial Remelting and Mechanical Stirring. *Trans. Nonferrous Met. Soc. China Engl. Ed.* **2010**, *20*, 1792–1798. [[CrossRef](#)]
11. Obeidi, M.; McCarthy, É.; Brabazon, D. A Review of Semi-Solid Aluminium-Steel Joining Processes. *AIP Conf. Proc.* **2016**, *1769*, 030005. [[CrossRef](#)]
12. Echaniz, E. Development of Hybrid Structures by Semi-Solid Forming of Aluminum of Steel. Ph.D. Thesis, Mondragon Unibertsitatea, Mondragón, Spain, 2016.
13. Liu, H.W.; Guo, C.; Cheng, Y.; Liu, X.F.; Shao, G.J. Interfacial Strength and Structure of Stainless Steel—Semi-Solid Aluminum Alloy Clad Metal. *Mater. Lett.* **2006**, *60*, 180–184. [[CrossRef](#)]
14. Cheng, Y.S.; Zhang, X.H. Interfacial Strength and Structure of Joining between 2024 Aluminum Alloy and SiCp/2024 Al Composite in Semi-Solid State. *J. Mater. Des.* **2015**, *65*, 7–11. [[CrossRef](#)]
15. Lozares, J.; Plata, G.; Hurtado, I.; Sánchez, A.; Loizaga, I. Near Solidus Forming (NSF): Semi-Solid Steel Forming at High Solid Content to Obtain as-Forged Properties. *Metals* **2020**, *10*, 198. [[CrossRef](#)]
16. Plata, G.; Lozares, J.; Sánchez, A.; Hurtado, I.; Slater, C. Preliminary Study on the Capability of the Novel near Solidus Forming (NSF) Technology to Manufacture Complex Steel Components. *Materials* **2020**, *13*, 4682. [[CrossRef](#)] [[PubMed](#)]
17. Slater, C.; Plata, G.; Sánchez, A.; Lozares, J.; Hurtado, I. A Novel Forming Technique to Coforge Bimetal Components into Complex Geometries. *Manuf. Lett.* **2020**, *26*, 21–24. [[CrossRef](#)]
18. Cheepu, M.; Seong, W. Influence of Friction Pressure on Microstructure and Joining Phenomena of Dissimilar Joints. *Trans. Indian Inst. Met.* **2020**, *73*, 1455–1460. [[CrossRef](#)]
19. Ding, Y.; You, G.; Wen, H.; Li, P.; Tong, X.; Zhou, Y. Microstructure and Mechanical Properties of Inertia Friction Welded Joints between Alloy Steel 42CrMo and Cast Ni-Based Superalloy K418. *J. Alloys Compd.* **2019**, *803*, 176–184. [[CrossRef](#)]
20. Mukherjee, T.; Debroy, T. Printability of 316 Stainless Steel. *Sci. Technol. Weld. Join.* **2019**, *24*, 412–419. [[CrossRef](#)]
21. Azpilgain, Z.; Ortubay, R.; Blanco, A.; Hurtado, I. Servomechanical Press: A New Press Concept for Semisolid Forging. *Solid State Phenom.* **2008**, *141–143*, 261–266. [[CrossRef](#)]
22. Becker, E.; Favier, V.; Bigot, R.; Cezard, P.; Langlois, L. Impact of Experimental Conditions on Material Response during Forming of Steel in Semi-Solid State. *J. Mater. Process. Technol.* **2010**, *210*, 1482–1492. [[CrossRef](#)]
23. Pierret, J.C.; Rassili, A.; Vaneetveld, G.; Bigot, R.; Lecomte-Beckers, J. Friction Coefficients Evaluation for Steel Thixoforging. *Int. J. Mater. Form.* **2010**, *3*, 763–766. [[CrossRef](#)]

Disclaimer/Publisher’s Note: The statements, opinions and data contained in all publications are solely those of the individual author(s) and contributor(s) and not of MDPI and/or the editor(s). MDPI and/or the editor(s) disclaim responsibility for any injury to people or property resulting from any ideas, methods, instructions or products referred to in the content.